Available online at www.sciencedirect.com
SCIENCE DIRECT®
Journal of Sound and Vibration 288 (2005) 981–1009
JOURNAL OF SOUND AND VIBRATION
www.elsevier.com/locate/jsvi

Interaction of unsteady separated flow over multi-bodies moving relatively in the same flow field

Sheng Zhou, Xin-qian Zheng*, An-ping Hou, Ya-jun Lu

Chinese National Key Laboratory of Aerodynamics & Thermodynamics of Aeroengine, Beijing University of Aeronautics and Astronautics, Beijing 100083, PR China

Received 6 January 2004; received in revised form 16 November 2004; accepted 14 January 2005
Available online 1 June 2005

Abstract

Unsteady separated flow is one of research frontiers in current aerodynamic. Great accomplishments have been acquired; however, most studies are on single body in a stream, such as studies on unsteady separated flows over airfoils. There are typical cases in the nature and engineering applications, in which several interacting bodies with relative motions are within the same flow field. These interacting unsteady separated flow fields not only are closely related to the phenomena of noise and flutter induced by flows, but also have strong influences on aerodynamic performances. With axial flow compressors as background, the present paper carried out studies on 'interaction of unsteady separated flow over multi-bodies moving relatively in the same flow field'. Experiment investigations carried out in the stationary annular cascade wind tunnel and the single-stage low-speed axial flow compressor experimental facility as well as relevant CFD simulations demonstrate that under properly organized interactions between all unsteady components, the time-space structure of unsteady separated flow field can be remarkably improved and the time-averaged aerodynamic performances be significantly enhanced accordingly. The maximum reduction of the loss coefficient reached 27.4% and 76.5% in the stationary annular cascade wind tunnel and the CFD simulation for single-stage axial flow compressor, respectively.

*Corresponding author. Tel.: +8610 82316624.
E-mail address: zhexq@hotmail.com (X.-q. Zheng).

0022-460X/$ - see front matter © 2005 Elsevier Ltd. All rights reserved.
doi:10.1016/j.jsv.2005.01.053

Nomenclature

$\vec{C}$	absolute velocity
C_r, C_θ, C_z	velocity components of $\vec{C}$
f_e	excitation frequency of upstream wake
$\bar{H}$	load coefficient; $\bar{H} = HL_u/\bar{U}^2$
i	incidence angle
k	load/loss ratio; $k = \bar{H}/\bar{\omega}$
L_u	work $L_u = \bar{U}(W_{\varphi 2} - W_{\varphi 1})$
Ma	Mach number
n	ordinal number
p	static pressure
p^*	total pressure
pl	total pressure loss; $pl = p^*_{\text{in}} - p^*_{\text{out}}$
q	arbitrary aerodynamic parameter
δq	relative change; $\delta q = (q_{\text{ex}} - q_{\text{un}})/q_{\text{un}} \times 100\%$
$\overline{\text{s.p.}}$	separate proportion coefficient; $\overline{\text{s.p.}} = \Delta S_{\text{sep}}/\Delta S$
ΔS	pitch of the cascade
ΔS_{sep}	width of the separated flow region in one ΔS
t	time
T	temperature
T^*	total temperature
$\bar{U}$	velocity of rotating
$\vec{W}$	relative velocity
W_r, W_φ, W_z	velocity components of $\vec{W}$
X	axial coordinate
Y	circumferential coordinate
Zs	number of stator blade
ρ	density
$\bar{\omega}$	loss coefficient; $\bar{\omega} = (p_1^* - p_2^*)/(p_1^* - p_1)$
θ	circumferential absolute coordinate
φ	circumferential relative coordinate
Ω	angular velocity of rotating

Subscripts

1	inlet
2	outlet
un	the condition of no excitation
ex	the condition of excitation

1. Introduction

One of the front areas in aerodynamic research is unsteady separated flow, which is further divided for the convenience of analysis on the basis of the number of bodies involved, as shown in Fig. 1.

In Fig. 1, both the flight formation of migratory birds during long-distance migration and the flow fields inside multi-stage axial flow compressors belong to the category of 'interaction of unsteady separated flow over multi-bodies moving relatively in the same flow field'. In addition, axial flow turbines, radial flow turbines and the layout of wind-driven turbine generators in a wind power plant are in the same category with many similarities. The present paper attempts to discuss how to properly organize interactions between inner unsteady separated flow fields, how to exploit the potentials imbedded in unsteady flow fields and how to improve their time-space structure to save energy.

Up to the sixties, all airfoils belonged to the first generation of attached steady flow type. Advancement in the aerodynamic performances of current fighter planes can be largely attributed to the application of the second-generation steady separated vortex flow type [1]. There are two common characteristics for these two generations of modern aeronautic flow types. First, only one body is considered in the flow field. Secondly, the assumption of steady flow is adopted. However, fluid dynamics covers a wide range of natural phenomena and engineering applications, many flow fields are not in accord with the above-mentioned characteristics. Hence a question arises as to whether the conception of flow type can still play an important role for those unsteady

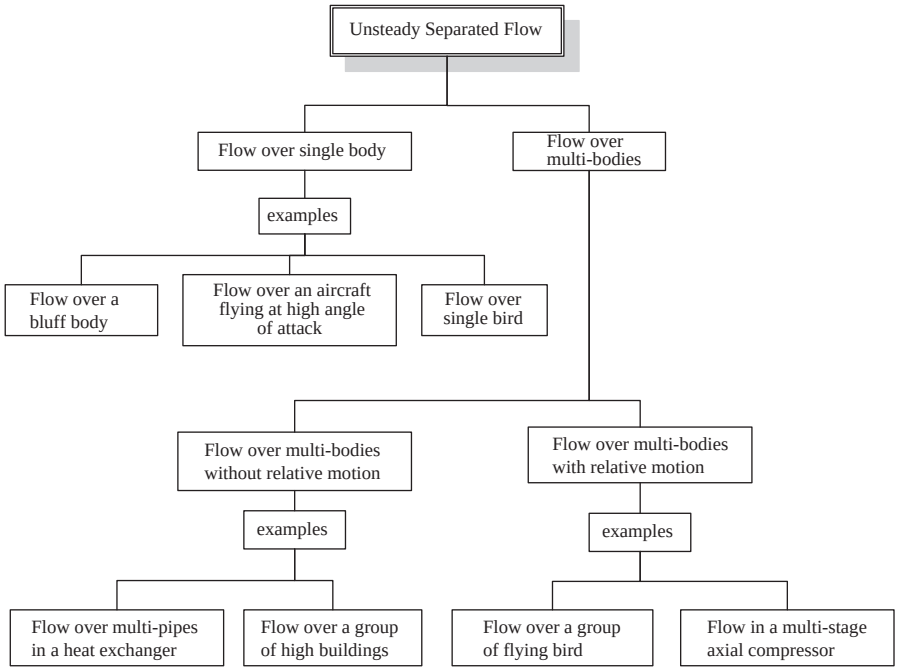

Fig. 1. Classification of the research on unsteady separated flow (based on bodies involved).

separated flow fields in which several relatively moving bodies with non-negligible interaction present?

By referring to the flight formation of migratory birds during long-distance migration, the present paper proposes in Section 2 a concept of two generations of unsteady separated flow types for the category of 'interaction of unsteady separated flow over multi-bodies moving relatively in the same flow field', which are named as 'unsteady natural flow type (UNFT)' and 'unsteady cooperative flow type (UCFT)'. In order to check and verify the above-mentioned concepts of UNFT and UCFT, the present research team carried out a series of experiments in planar cascade wind tunnel, stationary annular cascade wind tunnel and low-speed single-stage axial flow compressor experiment facility to capture UCFT and worked out relevant CFD simulations. The experiments of planar cascades for capturing UCFT were carried out in 2001 in China Gas Turbine Institute (located in Jiangyou city, Sichuan province). Positive and encouraging results were obtained in all these experiments and CFD simulations. Experiments in stationary annular cascade wind tunnels were carried out in 2003, experiment results and their comparison with related CFD results will be presented in Section 4. Experiments of single-stage low-speed axial flow compressors have not been completed yet; however, it could be concluded from intermediate experiment results that UCFT had been captured. Hence, only part of relevant CFD results will be given in Section 5. The experiments mentioned in Sections 4 and 5 are all carried out in our laboratory. All these experiments and related CFD based on reasonable physical and mathematical models will be first described in Section 3.

2. The concept of two generations unsteady flow types

2.1. Inspiration from the flight formation of migratory birds

The flight formation of migratory birds is a natural phenomenon widely studied. Ten species of migratory birds living in China was reported in Ref. [2] as flying in formations during long-distance migration. There may be many different reasons for flying in formation. Only one of them is the focus of the present paper, i.e. flying information can save lots of energy in comparison with flying individually [3,4].

The experiment was carried out for great white pelicans and presented in Ref. [3], in which the flight process was divided into two stages, i.e. wing beat stage and glide stage. The observation and measurement of Ref. [3] showed that, in comparison with flying individually, the heart rate of white pelican was reduced by 11.4–14.5% when flying in formation, resulting in less energy consumption. Except that the flight formation of migratory birds could save energy, the recent research shows that fish swimming in the same flock exploits the wake vortices of neighboring fish to decrease muscle activity [5,6].

2.2. Naming about two generations unsteady flow types

The measurement of Ref. [3] gave quantitative results for the first time on energy saving in migratory birds flying in formation, which contributed not only to zoology, but also to unsteady separated flow. In the region of unsteady separated flow research, 'interaction of unsteady separated flows over multi-bodies moving relatively' is classified as an independent category, because the unsteady excitations are forced by the wakes of surrounding bodies and impacting on the unsteady separated flow over the body under study. Since there is no need to have any external unsteady excitations, this is quite different from the study of individual airfoil under unsteady excitations. As for migratory birds flying in formation, from the viewpoint of controlling unsteady separated flows, the front row birds control downstream birds by means of their unsteady excitations, which can transform the time-space structures of flows over the latter, turning them from chaotic to coherent and orderly. Thus flows over migratory birds flying in formation can be classified into two flow types.

As for migratory birds flying in formation, an upstream flying bird forces unsteady excitations, if the frequency spectrum and amplitude of excitations are enough to bring about essential improvement to the time-space structure of flow over a downstream bird, then we may say the two birds, or the two flow fields, are coupled, and this flow pattern is named as 'unsteady cooperative flow type'. If migratory birds flying in formation are frightened and scattered, and then flying individually, excitations from other birds will not make distinct changes in the time-space structure of flows, which will remain chaotic. This flow pattern is named as 'unsteady natural flow type'.

2.3. Two generations unsteady flow types in axial flow compressors

Except for migratory birds flying in formation (and fish swimming in formation), axial flow compressor is also a typical case of 'interaction of unsteady separated flow over multi-bodies

moving relatively in the same flow field'. Alternately arranged stator blade rows and rotor blade rows are of course multi-bodies located in the same flow field. Even under design working condition, unsteady separated flows are inevitable. In order to visualize how much of the flow passage in the cascade is occupied by the separate flow region, a separate proportion coefficient for a blade element was defined in [7] as follows:

$$\overline{\text{s.p.}} = \frac{\Delta S_{\text{sep}}}{\Delta S}, \tag{1}$$

where ΔS is the pitch of the cascade, ΔS_{sep} the width of the separated flow region in one ΔS at the outlet of the cascade. A span-wise distribution of $\overline{\text{s.p.}}$ for a transonic fan rotor is shown in Fig. 2, from which severe separation near blade tip is obvious [8]. The separate proportion coefficient $\overline{\text{s.p.}}$ shows the blockage of flow passage by separation at the blade element [7].

Just as migratory birds fly in formation, there are two primary unsteady interacting factors in flows over each blade row of axial flow compressor. Firstly, there are inevitably local unsteady separated flows near blade tips. Secondly, the excitation effects of upstream rotating wakes on the time-space structure of unsteady separated flows over downstream blade rows. As for these flows, the attention is focused on the influence of unsteady wake of upstream body on the time-space structure of unsteady separated flow over downstream relatively moving body, which is called as 'Wake Impact Effects (WIE)'.

If the time-space structure of unsteady separated flow over downstream body does not show distinct modification under the impact of upstream wake, the corresponding flow type is named as 'unsteady natural flow type'.

Within a certain range of unsteady aerodynamic parameters, such as frequency spectrum, excitation intensity, the WIEs can significantly improve the time-space structure of unsteady separated flow over downstream body and greatly enhance its time-averaged performances, which one named as 'unsteady cooperative flow type'. For transforming UNFT into UCFT in axial flow compressors, the key mechanism is the couple of two frequencies, i.e. the frequency of upstream wake passing should be coupled with the characteristic frequency of vortex shedding in flow over

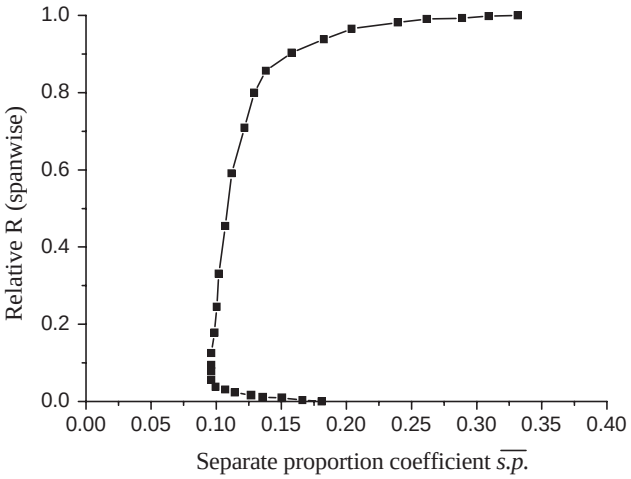

Fig. 2. Spanwise distribution of $\overline{\text{s.p.}}$ at trailing edge for a transonic fan rotor.

downstream adjacent rotor, resulting in the time-space structure of flow field changes from original chaotic state to coherent and more orderly.

As for axial flow compressors, modern aerodynamic design methods and analyses did not take this into consideration and flows inside compressors designed by steady aerodynamic methods are generally chaotic. Since UCFT will not occur by itself, the flow fields in modern axial flow compressors are basically UNFT. If we want them to be of cooperative flow Type, aerodynamic design method for unsteady separated flows must be adopted, which needs two necessary conditions. The first is the correct computation of the frequency spectrum and amplitudes of upstream wake impacts. The second is a correct understanding of the time-space structure of unsteady flows over the blade row under investigation. It means that a new kind of unsteady aerodynamics of separated flows must be adopted to design axial flow compressors.

If UNFT could be transformed into UCFT, it would be helpful for exploring the potential of unsteady flows in axial flow compressors and enhancing time-averaged performances, and it was proposed to make this a objective for the next generation unsteady aerodynamic design.

However, before UCFT was captured and verified, it was just a dream. In order to verify the concept of UNFT and UCFT, the present research team has carried out experiments in planar cascade wind tunnel, stationary annular cascade wind tunnel and low-speed single-stage axial flow compressor experimental facility as well as corresponding numerical simulations. This paper will present experimental results in stationary annular cascade wind tunnel and their comparison with related CFD results in Section 4. Experiments of single-stage low-speed axial flow compressors have not been completed yet; however, it can be concluded from intermediate experiment results that UCFT had been captured. Hence, part of relevant CFD results will be given in Section 5.

3. Related physical and mathematical models

3.1. Simplified model of single blade row

How to capture UCFT is essentially the problem of interaction between upstream stators and downstream rotors. However, it is not so easy to be implemented on single-stage low-speed axial flow compressor experimental facility, since it requires a series of geometric and aerodynamic parameters being changed, and it is also unfavorable for optimization analysis and studies on underlying mechanism for each separated factor. Therefore, a simplified model of single blade row is proposed in the present paper, in which the domain S/R is divided into sub-domain S and sub-domain R, and each sub-domain contains only one row of blades, as shown schematically in Figs. 3 and 4. The purpose of solving sub-domain S is to obtain unsteady inlet boundary conditions at the inlet boundary of sub-domain R, whereas the job of capturing new UCFT is possible with the solving of sub-domain R. In other words, the inlet boundary conditions of sub-domain R are used to represent the WIEs of the upstream blade row S on the downstream blade row R.

It can be seen from Fig. 4 that after the sub-domain S is removed, its effects must be represented by the boundary conditions at the boundary ‘in’ (inlet).

Therefore, the mathematical description and concrete expression of the unsteady inlet boundary conditions at the inlet boundary of sub-domain S are of key importance for the success of the simplified model of single blade row.

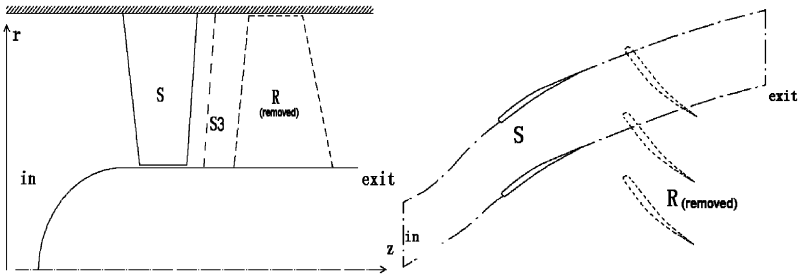

Fig. 3. Sketch of sub-domain S.

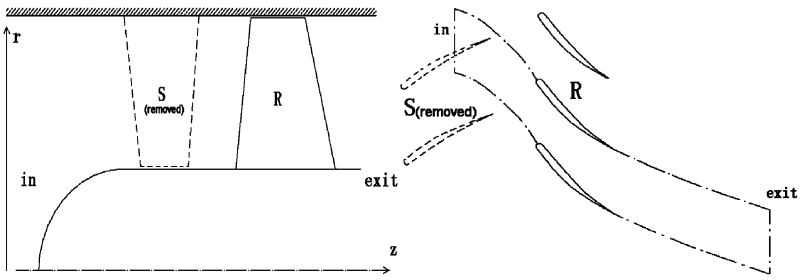

Fig. 4. Sketch of sub-domain R.

3.2. Mathematical description of single blade row model

3.2.1. Fourier expansion of aerodynamic parameters on the S3 surface in sub-domain S

The purpose of the present research is how to use WIE excitation of upstream stator to transform the flow type of the flow over downstream rotor, i.e. create the new UCFT. Hence, based on what is mentioned in Section 3.1, in solving sub-domain S, attention is focused on how to obtain the unsteady inlet boundary conditions at the inlet boundary of sub-domain R.

In actual construction, the axial size of domain is quite short, after it is divided into sub-domain S and sub-domain R, the two sub-domains must be extended at their outlet terminals, and their shapes are somewhat different from the actual ones as shown in Figs. 3 and 4. This is inevitable, since the static pressure at the exit are predetermined and kept unchanged with the variable θ; therefore, a S3 surface must be chosen from the CFD results of sub-domain S as shown in Fig. 3, on which aerodynamic parameters can vary with the variable θ. By means of steady CFD, the variation of all the aerodynamic parameters along the circumferential direction can be found and expressed as $q(\theta)$.

When considering the excitations imposed on the inlet boundary of sub-domain R, we can transform these aerodynamic parameters (functions of θ) on S3 surface of sub-domain S onto sub-domain R (in relative coordinate system), and the results are none other than the unsteady boundary conditions at the inlet boundary of sub-domain R.

First, it is assumed to be steady flow with periodic variable θ in circumferential direction:

$$q(\theta) = q\left(\theta + \frac{2\pi}{Zs}m\right), \tag{2}$$

where $1 \leqslant m \leqslant Zs$, Zs is the number of blade rows in the stator. Its Fourier expansion is as follows:

$$q(\theta) = \sum_{-\infty}^{\infty} C_m e^{imZs\theta}, \qquad m = 0, \pm 1, \pm 2, \ldots . \tag{3}$$

In S sub-domain, since the inverse pressure gradient will produce large separation, it will no longer be steady flow. The Fourier expansions of aerodynamic parameters on S3 surface should contain two variables θ and t.

Comparing it with the expansion (3), we get

$$q(\theta, t) = \sum_{m=-\infty}^{\infty} \sum_{n=-\infty}^{\infty} C_m^n e^{in\omega t} e^{imZs\theta}, \tag{4}$$

where ω stands for the main frequency in the frequency spectrum of the separated wake flow downstream of the stator, and

$$m = 0, \pm 1, \pm 2, \ldots .$$

3.2.2. Fourier expansion of aerodynamic parameters at inlet boundary of sub-domain R

The absolute coordinate system is transformed to the relative coordinate system by the following:

$$\theta = \varphi + \Omega t, \tag{5}$$

where Ω is angular velocity of the rotor (Ω is assumed to be a constant). Substituting Eq. (5) into Eq. (3), we get

$$\begin{aligned} q(\varphi, t) &= \sum_{m=-\infty}^{\infty} C_m e^{imZs(\varphi+\Omega t)} \\ &= \sum_{m=-\infty}^{\infty} e^{imZs\varphi} e^{imZs\Omega t}, \qquad m = 0, \pm 1, \pm 2, \ldots . \end{aligned} \tag{6}$$

Substituting Eq. (5) into Eq. (4), we obtain

$$\begin{aligned} q(\varphi, t) &= \sum_{m=-\infty}^{\infty} \sum_{n=-\infty}^{\infty} C_m^n e^{in\omega t} e^{imZs(\varphi+\Omega t)} \\ &= \sum_{m=-\infty}^{\infty} \sum_{n=-\infty}^{\infty} C_m^n e^{imZs\varphi} e^{i(mZs\Omega+n\omega)t}, \qquad m = 0, \pm 1, \pm 2, \ldots . \end{aligned} \tag{7}$$

Eq. (6) means that if there is no obvious vortex shedding in the wake of upstream stator in the absolute coordinate system, it can be considered as a steady flow, i.e. $\omega = 0$. In this case, at the inlet there are several self-rotating moving waves with an angular velocity of $|mZs\Omega|$ encircling the rotor in the relative coordinate system.

Eq. (7) means that if there is large-scale separated flow around the upstream stator, there will be obvious vortex shedding in the wake of upstream stator with main frequency of ω. In this case, at the inlet there are several self-rotating moving waves with an angular velocity of $|mZs\Omega + n\omega|$ encircling the rotor in the relative coordinate system. In comparison with Eq. (6), the rotating moving waves and rotating modes are obviously changed.

3.2.3. Concrete expressions of 3D unsteady inlet boundary conditions

As a preliminary study, the steady assumption is adopted for the sub-domain S. Based on the description of Sections 3.2.1 and 3.2.2, commercial software NUMECA is applied to obtain five basic physical variables $C_r, C_\theta, C_z, p, \rho$, i.e. their distribution along θ direction on S3 surface in an absolute coordinate system (they are directly solved in the governing equations, which, and definite conditions, are the same as used in routine approaches). These five variables are then transformed from the absolute coordinate system to the relative coordinate system, resulting in $W_r(t)$, $W_\varphi(t)$, $W_z(t)$, $p(t)$, and $\rho(t)$. Now the non-uniformity in space in absolute coordinate system is transformed into unsteadiness in time in relative coordinate system and all other physical variables at the inlet of sub-domain R, such as $T(t)$, $p_w^*(t)$, $T_w^*(t)$, $\rho_w^*(t)$, $Ma_w(t)$, and $\beta(t)$, can be obtained through algebra relations.

Based on the compatibility theory of 3D characteristics [9], under axially subsonic working conditions (this is true for all the existing compressors), four physical variables should be given at the inlet boundary and additional variable will be given by the compatibility condition. On the other hand, one variable should be given at the outlet boundary, and 4 variables will be given by the compatibility conditions.

Furthermore, it must be emphasized that at the inlet of sub-domain R, they are not only velocity amplitude fluctuations but also incidence fluctuations due to the transformation between the two coordinate systems, as shown in Fig. 5. The fluctuations of incidence is relatively more important than that of velocity amplitude, which means if there is a large scale separated flow around the upstream stator, it will not only cause loss in itself, but also influence the downstream cascade, since the latter will undergo instantaneous large incidence much longer. There is difficulty in the aerodynamic design of axial flow compressors—the interaction between various rows of blade, i.e. the interaction between domain R/S and domain S/R.

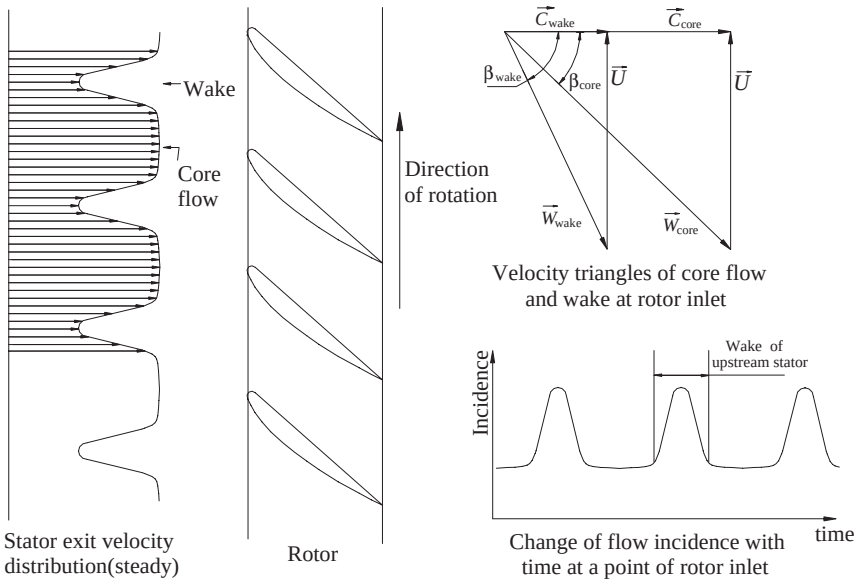

Fig. 5. Sketch of incidence fluctuations at the inlet of rotor.

The above-mentioned is an approximation, which adopted steady assumption for sub-domain S and is appropriate for the present experiments. Since our 3D CFD software has the capacity to compute separated flows, we can abolish the steady assumption for sub-domain S and adopt a more accurate model if necessary.

3.3. Acoustic excitations at unsteady inlet boundary for modeling WIE

We have presented the simplified model of single blade row and its mathematical description, given unsteady boundary conditions at rotor's inlet to represent WIE of the wake. However, it is not so easy to provide this kind of boundary conditions in experiments to model WIE, hence acoustic excitations are adopted to model actual WIE in axial flow compressors. The feasibility can be described as follows.

A theory of two generations unsteady flow types was presented in Section 2, the key can be summarized as follows. The unsteady separated flow of downstream rotor is influenced by the alternative passing of main flow and wake of upstream stator and the unsteady separated flow is then transformed from UNFT into UCFT, resulting in enhanced time-averaged aerodynamic performances. As for the rotor, the upstream wake is a kind of an unsteady excitation, the characteristic parameters of which are unsteady excitation frequency (frequency of wake passing) and unsteady excitation amplitude (amplitude of wake defect) mainly. Therefore, any kind of unsteady excitations with proper frequency and proper amplitude can be used to model WIE; at least can be used to check underlying mechanism. Acoustic excitation is convenient to apply to experiments, and is thus adopted. Although it cannot model all the effects of WIE, however, we believe it is feasible for testing underlying mechanism. Experiments of capturing UCFT by acoustic excitations in stationary annular cascade will be presented in Section 4.

4. Capturing UCFT in stationary annual cascade experimental facility

4.1. Description of stationary annular cascade wind tunnel

4.1.1. Construction of stationary annular cascade wind tunnel

The panorama of experimental facility is shown in Fig. 6, in which the inlet section is a lemniscate-horn-shape gas-contractor to make the flow uniform at the guiding ring, and there are four static holes on the straight section for measuring flow rate.

Guiding ring and diffusing cascade ring are shown in Figs. 7 and 8, the incidence of diffusing cascade blades is designed to be adjustable as shown in Fig. 9.

The main design parameters of the annular cascade facility are listed in Table 1.

4.1.2. Arrangement of acoustic excitations

External excitations are used for acoustic excitations, i.e. the excitations are transmitted through holes on the shroud from outside, instead of being produced at the surface of local blade. The excitations are imposed on the leading edge of diffusing blade as shown in Fig. 10. Furthermore, the cascade experiment facility is rotated to expose the blade under measurement to the sidewall to facilitate the installation of speaker on the shroud, as shown in Fig. 11. Holes are

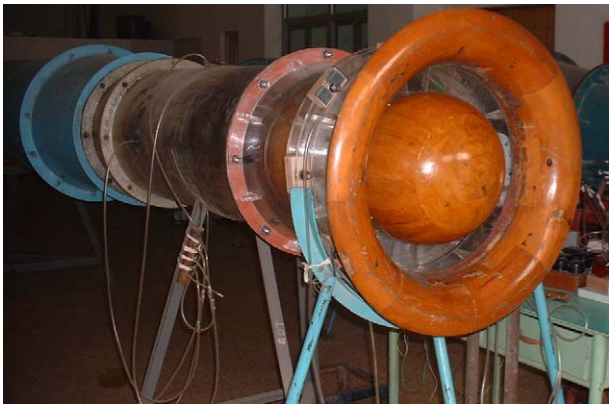

Fig. 6. Photo of the annular cascade.

Fig. 7. Guiding ring.

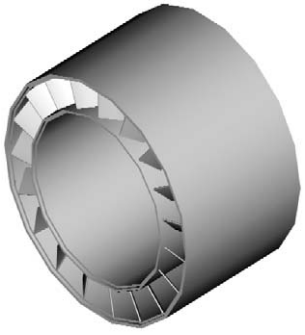

Fig. 8. Diffusing cascade ring.

drilled on the shroud with sizes suitable for the outlet of speaker's acoustic conduit, and it is thus convenient to introduce acoustic excitations into cascade flow field within the shroud.

Different excitation location may bring about different results; hence, slots are drilled on the shroud to shift the location for forcing excitation in Fig. 12.

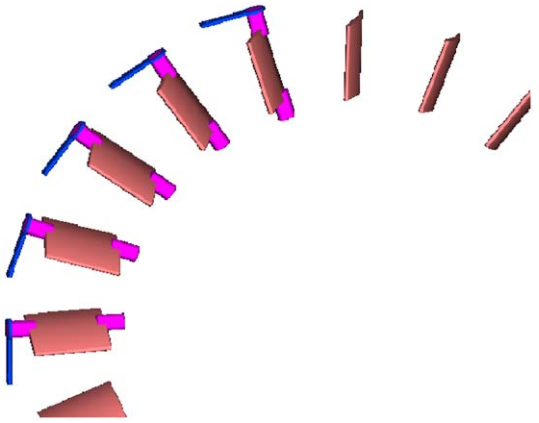

Fig. 9. Adjustable diffusing blade.

Table 1
Design parameters of the cascade facility

Outer diameter	450 mm
Blade height	56 mm
Chord length of compressor blade	56 mm
Chord length of guide vane	65 mm
Number of guide vanes	23
Number of compressor blade	19
Compressor blade pitch	65 mm
Mass flow	5 kg/s
Inlet Mach number	0.07
Reynolds number based on chord	1.07×10^5

4.1.3. Arrangement of PIV measurement and optical path

In order to obtain detailed information on flow-field structure, PIV technique is adopted, in which tracing particles are used to measure velocity field, and can be explained as follows. Small particles are introduced into and carried by the flow field; the displacements of particles in two or more time intervals are measured and velocities are calculated accordingly, which are assumed to be the local velocities of the flow field. The overall inaccuracy in PIV measurement is estimated to be lower than 5%.

First, appropriate lens are used to transform the laser beam emitted from a dual cavity Nd:YAG laser into a sheet of laser. The latter is, by means of a group of self-made planar mirrors, then introduced into the internal of compressor and sheds light on the flow field as shown in Fig. 13.

Charge-coupled devices are adopted in photographic system. Since the entire experimental section is made of plexiglass, there is no need to drill holes on the shroud for CCD photography and record, CCD camera can shoot or take photos through the plexiglass shroud.

Since the stationary cascade blades were made of plexiglass, severe optical reflections appeared, which would not only damage the CCD camera, but also distort the images severely. Therefore,

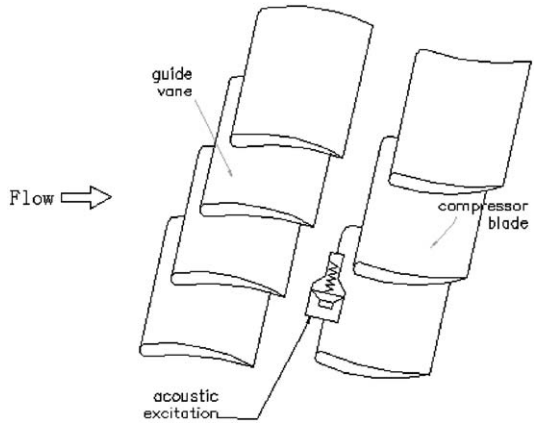

Fig. 10. Location for forcing acoustic excitation.

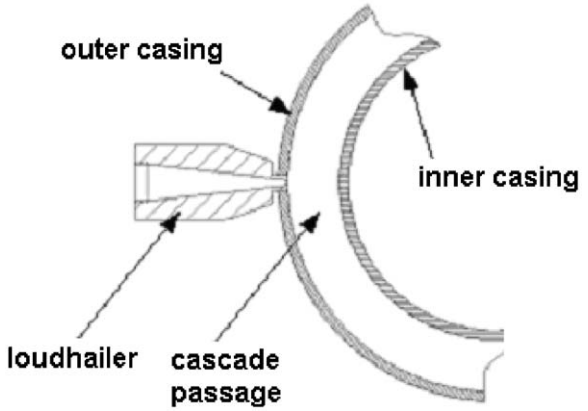

Fig. 11. Fitting of acoustic conduit with the shroud.

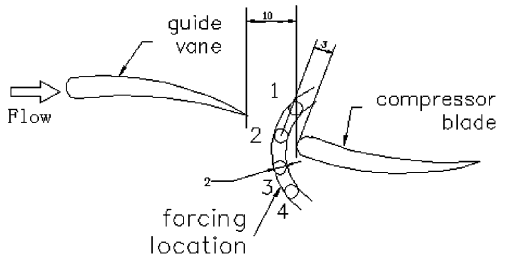

Fig. 12. Four locations for forcing acoustic excitation.

this became the key problem for successful application of PIV. After several trials, it was finally decided that the blades were first painted with black alkyd paint, then carbon powder was uniformly cast on its surface before it was dried, and finally redundant carbon powder was

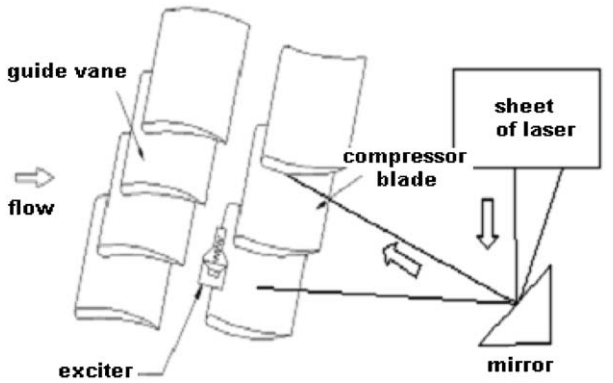

Fig. 13. Arrangement of optical path.

removed after the paint was dried. The finished blades were proved effective in preventing optical reflection and qualified for the experiments.

4.2. Experiment results and analysis

4.2.1. Using hot wire anemometer to measure the characteristic frequency of vortex shedding

The frequency of vortex shedding is measured in the flow over diffusing cascade. Frequency spectra at the incidence of -18.6°, -8.6°, 1.4° and 11.4° are shown in Fig. 14. The measurement shows that in the flow over diffusing cascade, the frequency of vortex shedding from the trailing edge on center stream section is 717.2, 718.9, 721.4 and 723.8 Hz, respectively. The results reveal that under constant flow rate and unchanged characteristic length of chord, the present diffusing cascade has a characteristic frequency of vortex shedding of nearly 720 Hz, which provides an extremely important characteristic frequency.

4.2.2. Influences of unsteady excitations on flow performances

With flow rate kept unchanged, a total pressure comb was used to measure time-averaged total pressure loss of the diffusing cascade under different incidences both with and without excitations, and the results were applied to analyze the influences of unsteady excitations on flow performances. For brevity, experiment results about the impacts of various parameters, such as excitation frequency, excitation intensity and excitation location, on flow performances will not be presented and discussed here, details can be found in Ref. [10]. The optimal parameters of the acoustic excitation are associated with the separated flow. In this paper, only the measured performances of UNFT are compared with that under the optimal excitation condition to illustrate the potential in improving compressor performances by means of transforming flow type.

A 13-hole total pressure comb is installed at the exit near the diffusing cascade trailing edge to measure time-averaged total pressure loss in a pitch behind the diffusing cascade. The installation location of the total pressure comb is shown in Fig. 15. The total pressure comb is 3 mm to the trailing edge, i.e. 5% of the chord length, measurement is carried out at the center radial section. Total pressure loss at different incidences without excitation is shown in Fig. 16.

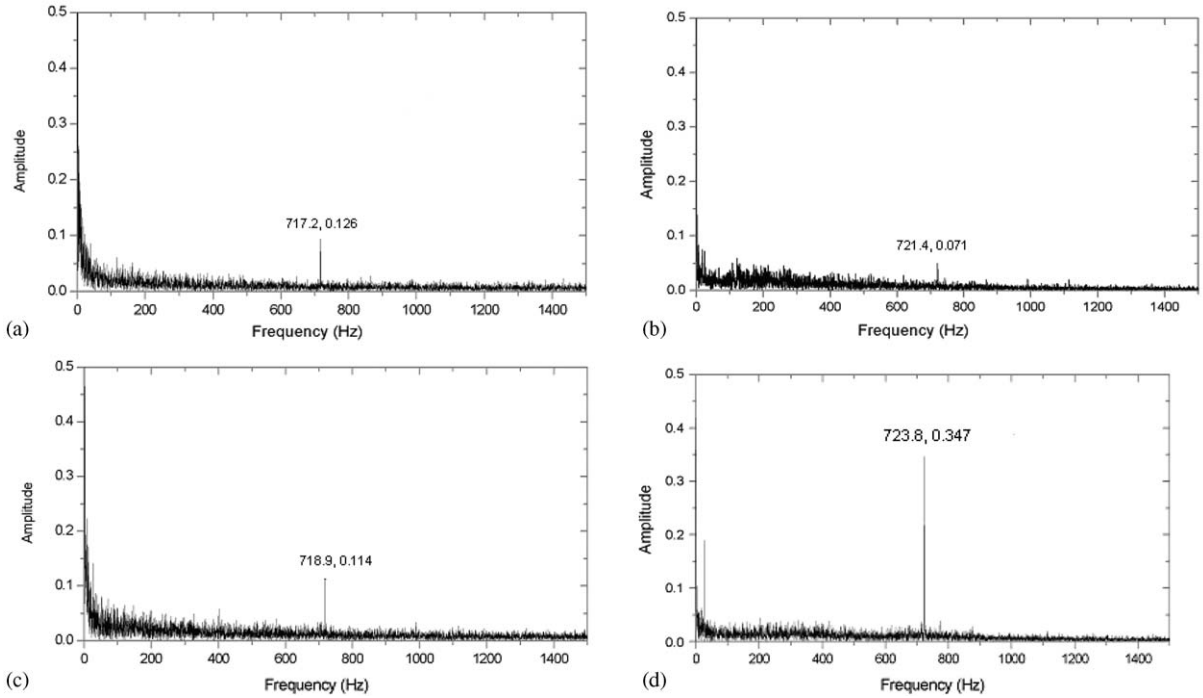

Fig. 14. Determination of the frequency of vortex shedding from trailing edge. (a) $i = -18.6^\circ$; (b) $i = -8.6^\circ$; (c) $i = 1.4^\circ$; (d) $i = 11.4^\circ$.

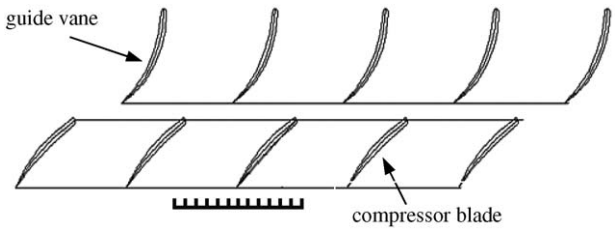

Fig. 15. Arrangement of pressure comb.

The frequency of vortex shedding at different incidence (about 720 Hz) is taken as the frequency of acoustic excitation, the acoustic excitation is introduced at the leading edge of blade and the power of loudspeaker is about 35 w. The distributions of total pressure loss along the pitch direction at incidence of 10° and 15° with and without excitation are shown in Figs. 17 and 18. With excitation, imposed, the total pressure loss in wake region is reduced significantly. The reduction percentage of loss coefficient with excitation is calculated for 7 incidences and denoted as $\delta\bar{\omega}$, its relation with incidence is derived and shown in Fig. 19. It is obvious from Fig. 19 that within a wide range of incidence, after the imposed excitation turns UNFT into UCFT, the loss coefficient is greatly reduced and the aerodynamic performance of the flow field is improved significantly. At an incidence of $i = 15^\circ$ and under the optimal excitation condition, the reduction

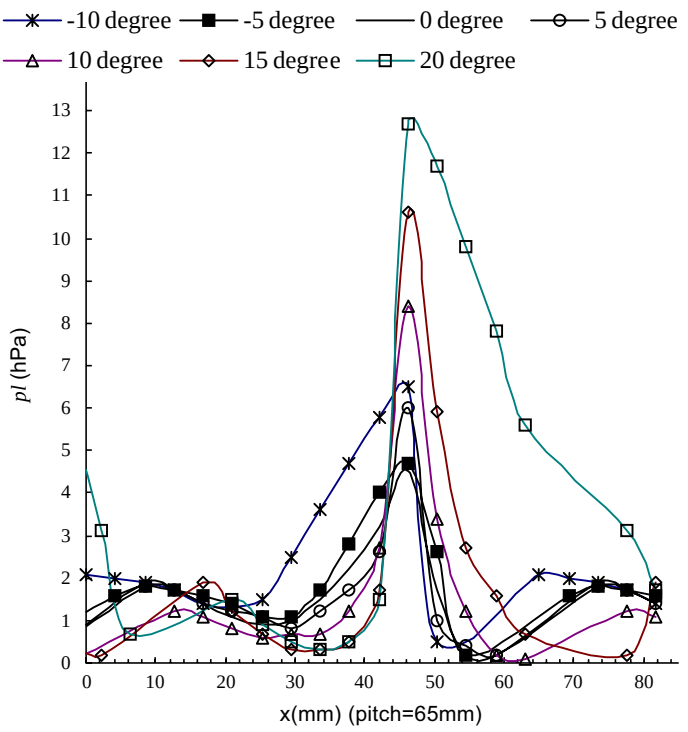

Fig. 16. Total pressure loss at different incidences.

of total pressure loss reaches 27.4%, which fully illustrates the enormous potential that may be gained when properly organized unsteady excitation of wake impact (WIE) turns UNFT into UCFT inside axial flow compressors.

4.2.3. Using PIV technique to measure the change of time-space structure of flow field

We have presented positive results of improved aerodynamic performances, now we turn to the corresponding change of the time-space structure of flow field [11]. Instantaneous vorticity field and streamlines measured by PIV are shown in Fig. 20, in which the shade of color represents the intensity of vorticity, blue stands for wake vortex (negative vorticity, clockwise) and red stands for separated vortex (positive vorticity, counterclockwise).

Inlet flow rate kept unchanged, instantaneous vorticity field and streamlines measured at different incidences without excitation are shown in Fig. 21, in which the existence of wake vortices is clearly displayed. As the incidence increases from 5° to 18°, streamlines become more and more twisted and chaotic and the separation area becomes larger and larger. Meanwhile, the intensity of wake vortices becomes stronger and the wake spreads wider, particularly when the incidence exceeds 16°, the distribution of vorticity intensity becomes much more chaotic. This means that as the incidence increases, the flow field becomes more and more chaotic and the separation becomes more and more severe.

With inlet flow rate unchanged, instantaneous vorticity field and streamlines measured at different incidences with excitation are shown in Fig. 22, in which the existence of wake vortices is

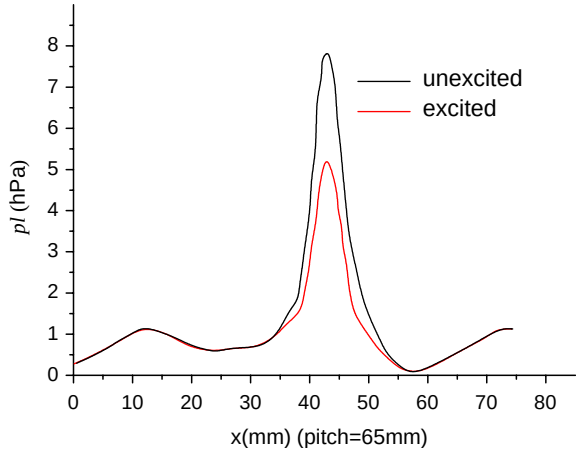

Fig. 17. Total pressure loss with excitation , $i = 10°$.

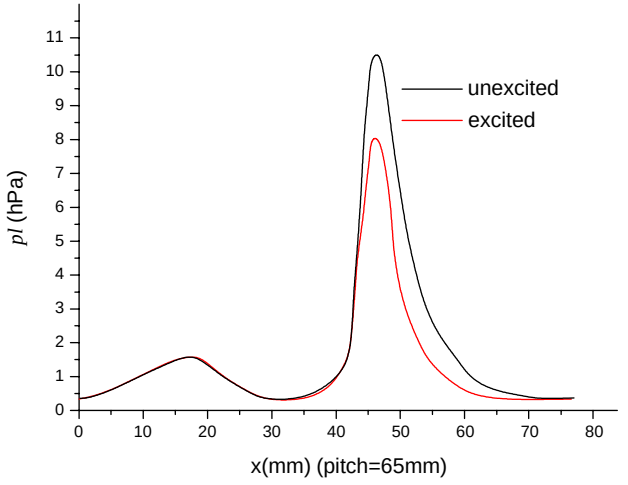

Fig. 18. Total pressure loss with excitation , $i = 15°$.

clearly displayed. It is obvious from its comparison with Fig. 21 that the intensity of wake vortices becomes much weaker with excitation imposed and streamlines become smoother and more uniform. After turning from UNFT into UCFT by unsteady excitation, the enhancement of overall performance of flow field is the result of the improvement of the time-space structure of flow field. These comparisons provide some evidence of capturing UCFT in the experiments.

The time-space structure of unsteady separated flows can be divided into two types, one is to describe the spatial structure of flow field at any fixed time, another is to describe the time variation of flow field at any given point. The figures obtained by the PIV technique belong to the former, whereas the latter chiefly uses frequency spectrum, and we will not go into details here for brevity.

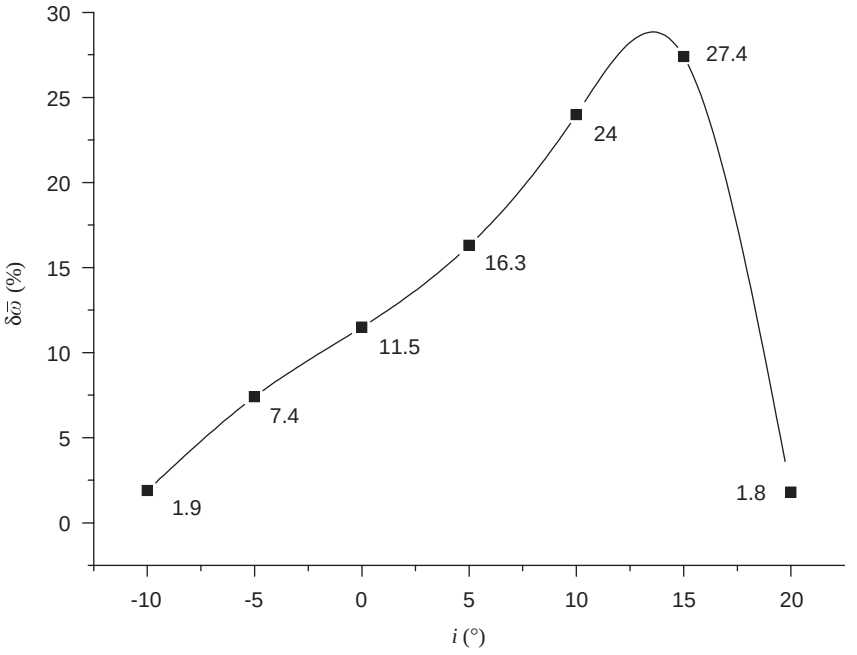

Fig. 19. Relative reduction of loss coefficient vs. incidence.

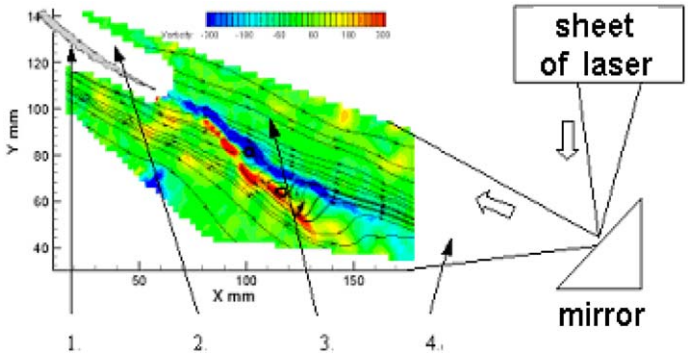

Fig. 20. Introduction of the picture by PIV (color shade represents vorticity intensity). (1) Profile of diffusing cascade; (2) eliminated part for avoiding interference of black light; (3) streamlines; (4) laser sheet after reflecting from planar mirror.

4.3. Relevant numerical simulation

Experiments carried out in stationary annular cascade wind tunnel have obtained positive results with regard to capturing UCFT, and have been verified by PIV measurement. The enhancement of overall performance of flow field is closely related to the improvement of the time-space structure of flow field. In addition, related numerical simulations are also carried out [12], in which the governing equations are Reynolds-averaged viscous unsteady N–S equations.

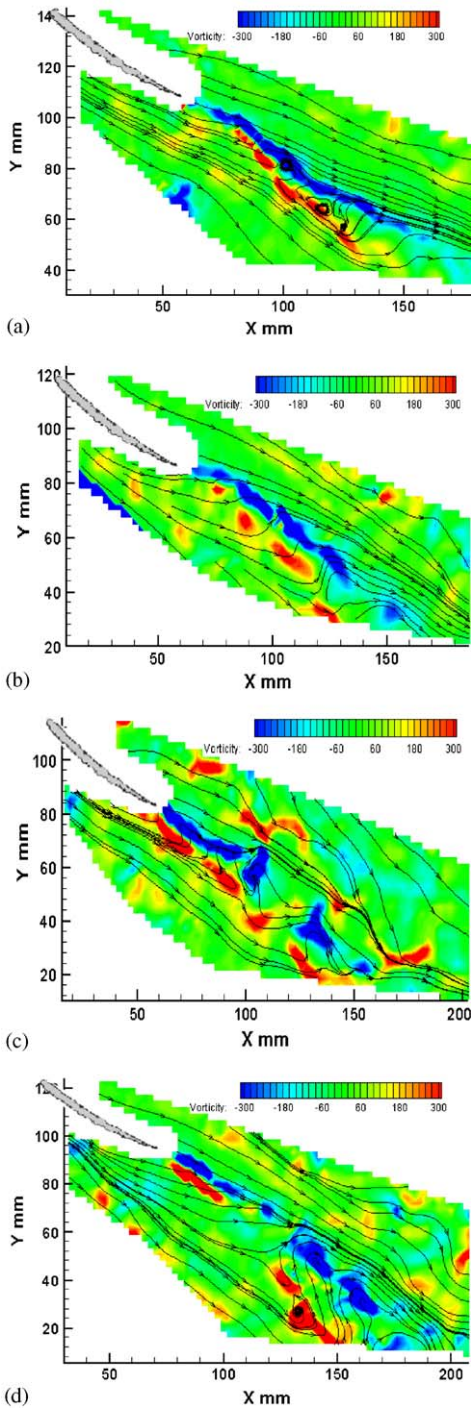

Fig. 21. Instantaneous vorticity field and streamline by PIV without acoustic excitation. (a) $i = 5^\circ$; (b) $i = 10^\circ$; (c) $i = 16^\circ$; (d) $i = 18^\circ$.

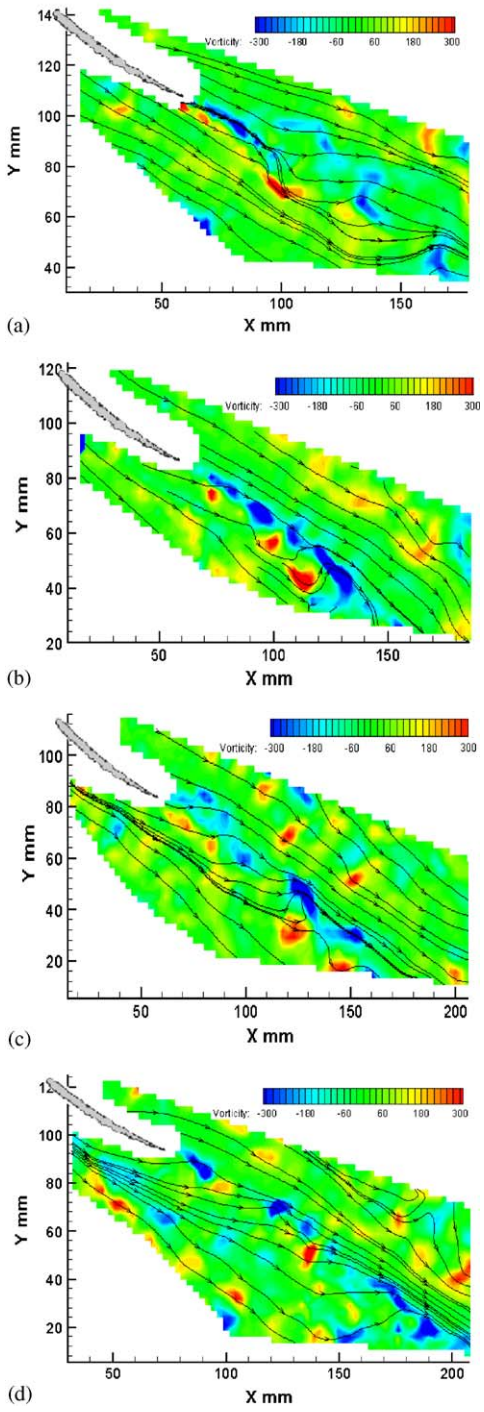

Fig. 22. Instantaneous vorticity field and streamline by PIV with acoustic excitation. (a) $i = 5^\circ$; (b) $i = 10^\circ$; (c) $i = 16^\circ$; (d) $i = 18^\circ$.

For brevity, the procedure involved and large amount of results will not be presented in detail, only some computed vorticity fields are compared with those measured by PIV technique.

Instantaneous vorticity field and streamlines measured with and without excitation are shown in Figs. 23 and 24. The incidence is chosen at $i = 10^\circ$ randomly. Conclusion can be drawn from the comparison of these two figures that the separation area behind blade is shrunken, the vorticity intensity is greatly reduced and the structure of flow field is improved; although the measured vorticity fields and streamlines are somewhat different from those obtained by

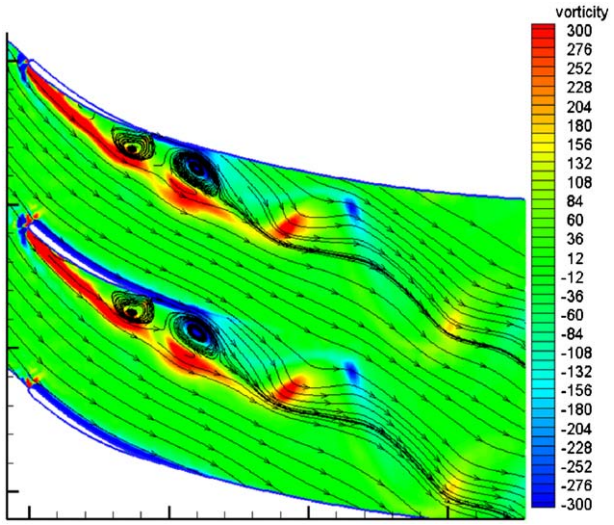

Fig. 23. Instantaneous vorticity field and streamline at $i = 10^\circ$ by computation without excitation.

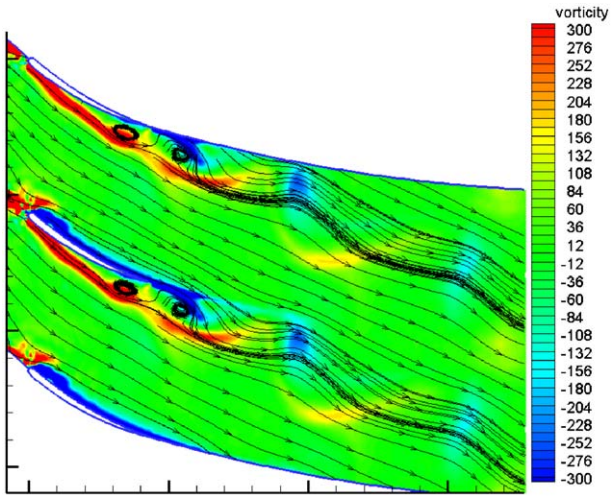

Fig. 24. Instantaneous vorticity field and streamline at $i = 10^\circ$ by computation with excitation.

simulation. However, when excitation is imposed, their changes and trends are consistent, both show reduced vorticity intensity, more orderly flow field and improved time-space structure of flow field. The similar rules are obtained at other incidences.

5. Capturing UCFT in low-speed axial flow compressor

Experiments of capturing UCFT in stationary annular cascade have been presented, in which acoustic excitation is used to model the WIEs. Actual interaction between stator and rotor is modeled in experiments carried out on single-stage low-speed axial flow compressor experiment facility, as shown in Fig. 25. The main parameters are listed in Table 2.

Experiments are still under way, however, the intermediate results showed that UCFT was preliminarily captured. Only part of the simulation results is presented here.

We have already presented how to capture UCFT in a single-computation domain in Section 3, the key step of which is the determination of unsteady inlet boundary conditions, which is used to represent reasonably the influences of upstream wake on downstream rotor. With the help of this model, numerical simulations of 3D low-speed axial flow compressors are carried out for capture UCFT.

5.1. Numerical scheme

Governing equations are 3D unsteady viscous Reynolds-averaged N–S equations. A third-order TVD Runge–Kutta time-marching scheme was used for time integration. Fifth-order accurate generalized compact scheme is used for spatial difference of inviscid fluxes. Simple B-L model is adopted as turbulence model.

Mesh in computation domain is produced by commercial software NUMECA, mesh points are 180 (stream-wise) × 50 (circumferential direction) × 40 (radial direction). A parallel computation

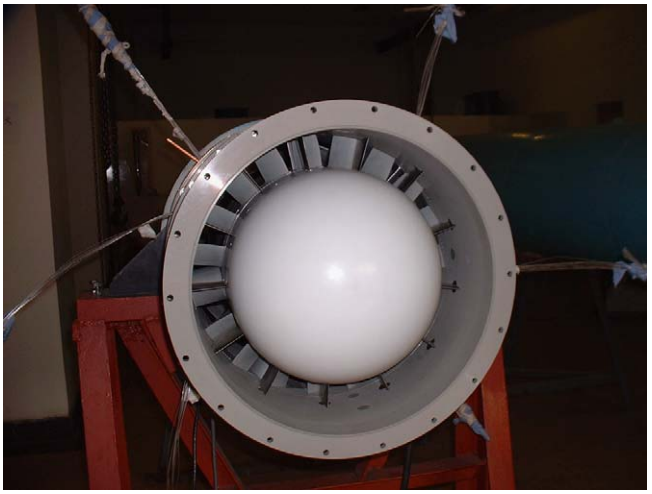

Fig. 25. Experimental section of the low-speed axial flow compressor experimental facility.

Table 2
The design parameters of the compressor

Outer diameter	450 mm
Number of guide vanes	13
Number of rotor blade	19
Number of stator blade	13
Rotor chord length at mid span	52 mm
Rotor blade pitch at mid span	65 mm
Rotor blade height	56 mm
Rotational speed of rotor	3000 rpm
Mass flow	2.88 kg/s
Compressor stage pressure ratio	1.015
Compressor stage efficiency	85%
Hub-tip radius ratio	0.75

Table 3
Comparison of computational and experimental results and design parameters

	Flow rate	Pressure ratio	Efficiency (%)
Design parameter (stage)	2.88	1.015	85
Experiment (stage)	2.80	1.015	86
Computation (single rotor)	2.82	1.0123	92

system with 26 linking points is adopted; the main feature of each linking point is CPU P4 2.4G, 512M memory. Each computation case requires 300 non-dimensional time steps, and takes about 70 h.

Since this is unsteady computation, results are time-averaged after the computation is converged. Comparison of computational and experimental results and design parameters is given in Table 3.

It can be concluded that the flow rate and efficiency are in agreement, the computed pressure ratio is somewhat lower than experimental result, and its stream-wise distribution is reasonable as shown in Fig. 26. The comparison demonstrates that the present program adopted for single rotor simulation is practical and feasible.

5.2. *Numerical simulation results of unsteady separated flows and analysis*

It is mentioned in Section 2 that for turning UNFT into UCFT in axial flow compressors, the key mechanism is the couple of two frequencies, i.e. the frequency of upstream wake passing should be coupled with the characteristic frequency of vortex shedding in flow over downstream adjacent rotor, and then the objective of controlling unsteady separation and enhancing time-averaged aerodynamic performances would be attained. Therefore, the computation can be divided into two steps. The first is to obtain the characteristic frequency of vortex shedding in flow over rotor under steady inlet boundary conditions and to calculate time-averaged aerodynamic

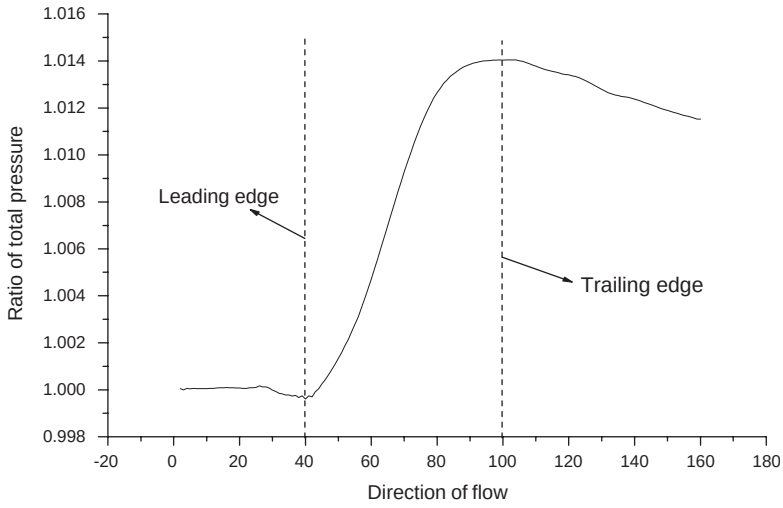

Fig. 26. Stream-wise distribution of pressure ratio under steady boundary condition.

performances. The second step, using this frequency and unsteady inlet boundary conditions given in Section 3.2.3, is to simulate the rotor's flow field structure under the excitation of different frequencies of wake passing, and to calculate the change of the corresponding time-averaged aerodynamic performances.

In order to obtain the characteristic frequency of vortex shedding, analysis of dynamic entropy contours is carried out in combination with the analysis of frequency spectrum of total pressure at different points in flow field. First, the location, intensity and rough period of the vortex shedding are obtained from the animation demonstration of entropy contours, the frequency of vortex shedding can thus be estimated. In the meantime, several points are selected for observing the total pressure to collect time-sequential values of total pressure at these points. The frequency spectrum of total pressure can thus be derived by operating fast Fourier transformation (FFT) on these time sequential values. The frequency of vortex shedding is obtained through analyzing this frequency spectrum, as shown in Fig. 27. If the estimated frequency from animation demonstration is basically consistent with that obtained from total pressure frequency spectrum, the location, intensity and frequency of the vortex shedding can be considered as correct and determined. By means of frequency spectrum and animation demonstration, we could affirm that the characteristic frequency of vortex shedding from trailing edge in relative coordinate system is nearly 3000 Hz.

After the time-space structure of flow field and characteristic frequency are obtained, now the interaction between the wake of upstream stator and the downstream flow fields is to be simulated, with the unsteady inlet boundary conditions given as in Section 3.2.3.

The influences of different frequencies of stator passing on the total pressure ratio of downstream adjacent rotor is shown in Fig. 28, more information is given in Table 3, in which the first row is aerodynamic performance without excitation and is taken as the standard for comparing enhanced performance under different excitation. It can be concluded from Fig. 28 and Table 3 that load coefficient does not change much (relative change is about 3–6%), whereas

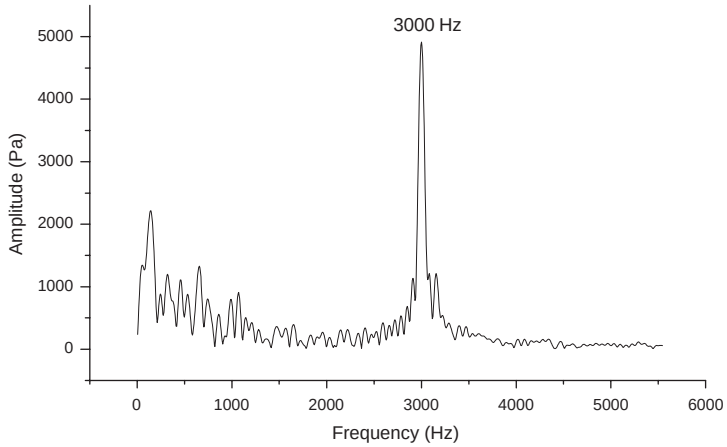

Fig. 27. Frequency spectrum of total pressure at certain point inside wake.

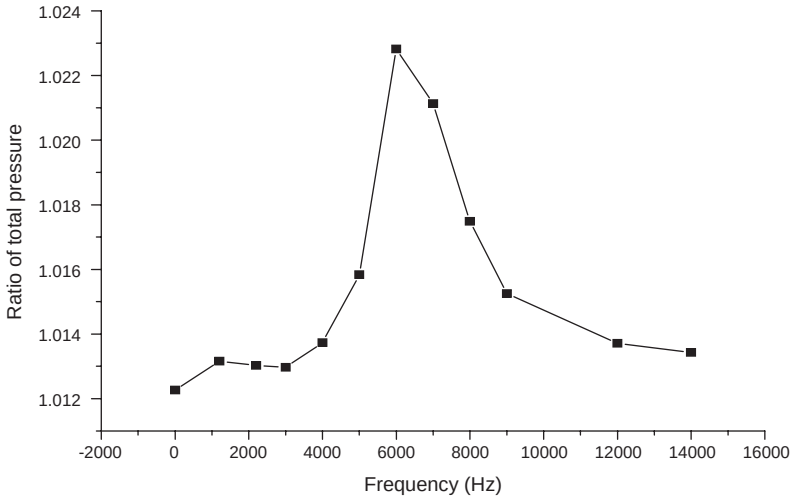

Fig. 28. Total pressure ratio under different excitation frequency.

the pressure ratio and loss coefficient are dramatically improved. The improvement of flow-field structure comes chiefly from the fact that the portion of added work by blade transformed into heat energy is reduced, and the efficiency of rotor is thus enhanced. The performance does not show monotonic increase with frequency. It reaches a peak and then drops to the original value, and the optimal frequency is just the double of the characteristic frequency of vortex shedding (6000 Hz). Therefore, reasonable organizing frequency of wake passing can enhance the aerodynamic performance of flow over downstream rotor, and the corresponding flow should be UCFT that we are pursuing (Table 4).

We found in this table that under certain conditions there occurred minus loss coefficients and the corresponding efficiency was greater than 1.0. As for the reason underlying $\bar{\omega} < 0$, we have not

Table 4
The influence of frequency of stator passing on time-averaged performances

f_e (Hz)	$\bar{H}$	$\bar{\omega}$	k	$\delta\bar{H}$ (%)	$\delta\bar{\omega}$ (%)	δk (%)
Unexcitation	0.032	0.119	0.269	0	0	0
1200	0.033	0.107	0.308	3.1	−10.1	14.5
2200	0.033	0.111	0.297	3.1	−6.7	10.4
3000	0.033	0.108	0.306	3.1	−9.2	13.8
4000	0.033	0.094	0.351	3.1	−21.0	30.5
5000	0.033	0.028	1.179	3.1	−76.5	338.3
6000	0.033	−0.175	—	3.1	—	—
7000	0.033	−0.143	—	3.1	—	—
8000	0.034	−0.016	—	6.2	—	—
10000	0.034	0.046	0.739	6.2	−61.3	174.7
12000	0.033	0.084	0.399	3.1	−29.4	48.3
14000	0.033	0.098	0.337	3.1	−17.6	25.3

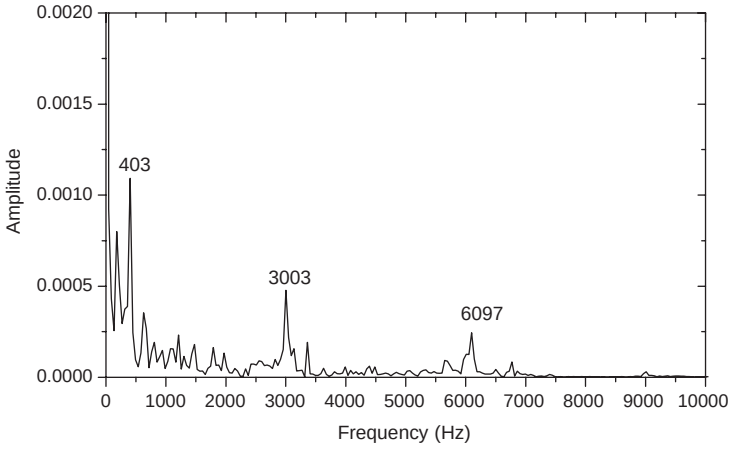

Fig. 29. Frequency spectrum of moment acting on blade surface under steady boundary condition.

got satisfactory answers. After preliminary studies, we thought the reason might be as follows. The traditional definition system of aerodynamic performance is established for steady non-separated flows, whereas our objective is now unsteady separated flows. The traditional definition cannot distinguish usable energy and unusable energy in unsteady flow field, and neglects the potential of energy transformation in unsteady flows.

Positive results have been obtained in numerical simulations of low speed axial flow compressors. When the frequency of upstream wake passing is unsteadily coupled with the characteristic frequency of vortex shedding from rotor, the time-averaged aerodynamic performances of rotor are enhanced. In order to understand the details of flow field and explore the mechanism underlying the improvement of aerodynamic performances, analysis is carried out for the frequency spectrum of moment acting on blade surface. The frequency spectrum of moment under steady and uniform boundary condition is presented in Fig. 29. The frequency spectrum of

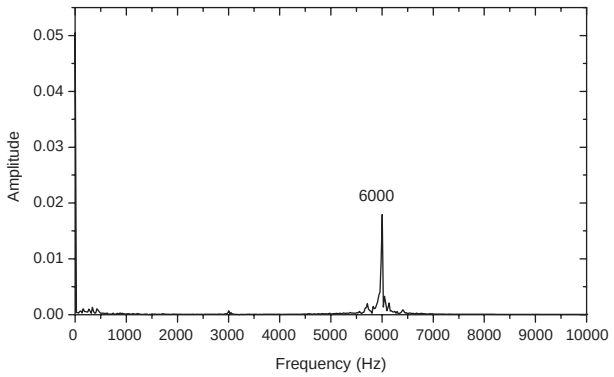

Fig. 30. Frequency spectrum of moment acting on blade surface under excitation of 6000 Hz.

moment under excitation (excitation frequency of 6000 Hz) is shown in Fig. 30. Conclusion can be drawn from the comparison that the characteristic frequency of 6000 Hz is most prominent, whereas other frequencies are effectively constrained. This phenomenon shows that the time-space structure of unsteady separated flow is transformed towards less chaotic and more orderly.

We note that the optical excitation frequency is equal to the vortex-shedding frequency in the stationary annular cascade experiments, while in the case of the single-stage axial compressor simulation the excitation frequency required for optimal performance is twice the vortex-shedding frequency. The discrepancy is due to the difference of unsteady excitation manner. The former is acoustic excitation that is only amplitude fluctuations, whereas the latter is forced by real wake of upstream vanes. There are not only velocity amplitude fluctuations but also incidence fluctuations due to the transformation between the two coordinate systems (referring to Fig. 5 and Section 3.2.3). The fluctuations of incidence are relatively more important than that of velocity amplitude. Further physical mechanisms need to be exploited in future.

6. Concluding remarks

(1) Unsteady separated flow is one of the front research areas in modern aerodynamics. Within the regime of unsteady separated flows, the category of 'interaction of unsteady separated flow over multi-bodies moving relatively in the same flow field' is different with other categories in Fig. 1. The main characteristics can be summarized as the unsteady excitations forced by the wakes of surrounding bodies and impacting on the unsteady separated flow over the body under study. When these excitations are strong enough to bring about essential transformation of the time-space structure of unsteady flow over the body from chaotic to coherent and more orderly, it is called 'unsteady cooperative flow type (UNFT)', otherwise it will be called 'unsteady natural flow type (UNFT)'.

As to unsteady separated flow inside axial flow compressor, the above-mentioned is displayed in the unsteady excitations of upstream blade wake flows on the time-space structure of unsteady separated flow over relatively moving downstream blade rows, which is called as 'wake impact effects' in the present paper.

(2) Viewing aerodynamic design of axial flow compressors from the standpoint of 'unsteady cooperative flow type', these methods can be classified into three types: (a) Steady aerodynamic design and analysis methods. Since wake impacts have not been taken into consideration, there will only be UNFT inside axial flow compressor, which means the potential of instantaneous random fluctuated flowing energy have not been utilized. (b) Unsteady aerodynamic design and analysis methods. The realization of unsteady cooperative flow type needs two necessary conditions. First, we must be able to compute correctly the time-space structure of unsteady flows over downstream blade row under investigation. Second, we must be able to compute correctly the frequency spectrum and amplitudes of unsteady wake excitations of upstream blade row. However, most unsteady methods cannot meet the above requirements. (c) Unsteady aerodynamic design and analysis methods. They are guided by unsteady cooperative flow type, which can meet the above two necessary conditions.

From the comparison of these three kinds of design methods, if WIEs inside axial flow compressor are to be used for transforming the time-space structure of unsteady separated flow from chaotic to coherent and orderly, the third kind of design methods must be applied and the realization of unsteady cooperative flow type should be taken as the objective of the design.

(3) For testing the concept of two generations unsteady flow types in axial flow compressors, experiments were carried out in planar cascade wind tunnel, stationary annular wind tunnel and low-speed single-stage axial flow compressor experimental facility together with related CFD simulations. UCFT was captured in all these three sorts of experiments. Parts of experiment and simulation results are presented, together with adopted physical and mathematical models.

With the help of simplified model of single blade row, UCFT was captured in both the experiments of stationary annular cascade and the experiments of single-stage low-speed axial flow compressor. The experiments of stationary annular cascade and related simulations as well as the CFD results of single-stage low-speed axial flow compressor demonstrated that, within a certain range of unsteady parameters, such as frequency and excitation intensity, the WIEs can significantly improve the time-space structure of the unsteady separated flows over downstream bodies, shrink separation area behind the blade and weak vorticity intensity, resulting in more smooth and more uniform streamlines, more coherent time-space structure and enhanced time-averaged performances of unsteady flow fields. In the experiments carried out in stationary annular cascade wind tunnel, the maximum relative reduction of loss coefficient was 27.4%, whereas in CFD simulation of single-stage low-speed axial flow compressors, the reduction of loss coefficient reached 76.5%. It might be concluded that the theory of two generations unsteady flow types for axial flow compressors was preliminarily validated at the level of basic research.

Acknowledgments

This paper is funded by National Nature Science Foundation of China (No. 10477002 & No. 10072008) and the Research Fund for the Doctoral Program of Higher Education (2000000615).

References

[1] D. Kuchemann, *The Aerodynamic Design of Aircraft*, Pergamon Press, Oxford, 1978.
[2] T.H. Cheng, *Economic Birds in China*, second ed, Science Press, Beijing, China, 1993 (in Chinese).
[3] H. Weimerskirch, J. Martin, Y. Clerquin, P. Alexandre, S. Jiraskova, Energy saving in flight formation, *Nature* 413 (2001) 697–698.
[4] J.M.V. Rayner, Fat and formation in flight, *Nature* 413 (2001) 685–686.
[5] J.C. Liao, D.N. Beal, G.V. Lauder, M.S. Triantafyllou, Fish exploiting vortices decrease muscle activity, *Science* 302 (2003) 1566–1569.
[6] U.K. Müller, Fish 'n flag, *Science* 302 (2003) 1511–1512.
[7] X.Q. Xing, J. Zhang, S. Zhou, A method to determine block coefficient from test loss coefficient, *Experiments & Measurements in Fluid Mechanics* 13 (2) (1999) 10–15.
[8] X.Q. Xing, S. Zhou, X.L. Zhao, A methodology to relate blockage coefficient to test loss coefficient in a transonic axial compressor *2nd ISFMFE*, Invited Lecture, October 22–25, Beijing, 2000, pp. 18–23.
[9] M.Y. Shen, S. Zhou, B.Z. Lin, *Transonic flow in turbomachinery, Chapter 4: Discussion on Boundary Conditions in Time-Matching Method, in Series of Mechanics*, Science Press, Beijing, China, 1988 pp. 84–112 (in Chinese).
[10] Y.X. Qiu, J.D. Ge, Y.J. Lu, S. Zhou, Q.S. Li, Research on sound-vortex resonance in enhancing performance of an annular cascade, ASME GT2003-38022, 2003.
[11] J.D. Ge, An Experimental Investigation on the Structure of the Separated Flow Field in a Static Annular Cascade by Using PIV, Degree thesis, Beijing University of Aeronautics and Astronautics, Beijing, China, 2003 (in Chinese).
[12] W. Tuo, Structure Analysis on Unsteady Separated Flow in Axial Compressor Blade Row, Degree thesis, Beijing University of Aeronautics and Astronautics, Beijing, China, 2003 (in Chinese).